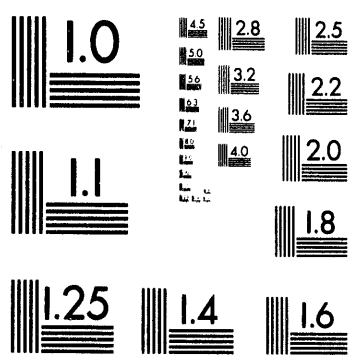
1.0
1.1
1.25
1.4
1.6
1.8
2.0
2.2
2.5
2.8
3.2
3.6
4.0
4.5
5.0
5.6
6.3
7.1
8.0
9.0

1 of 1

ANL/CHM/PP--75303

ION DOSE DEPENDENCE OF THE SPUTTERING YIELD: Ar^+, Ne^+, and Xe^+ BOMBARDMENT OF Ru(0001)AND Al(111)

J. W. Burnett,† M. J. Pellin, J. E. Whitten, D. M. Gruen
Materials Science/Chemistry Divisions
Argonne National Laboratory
Argonne, IL 60439

J. T. Yates, Jr.
Surface Science Center/Department of Chemistry
University of Pittsburgh
Pittsburgh, PA 15260

DISCLAIMER

*Work supported by the U. S. Department of Energy, BES-Materials Sciences, under Contract W-31-109-ENG-38.

Abstract

The sputtering yield from clean metal surfaces has long been considered to be insensitive to primary ion dose at moderate ion fluences ($< 10^{18}$ ions/cm^2). Using carefully cleaned and well-characterized targets, the ion dose dependence of the sputtering yield of Ru(0001) and Al(111) has been investigated. The sputtering yield of Ru(0001) is found to decrease substantially following primary ion bombardment at low fluences, while the sputtering yield of Al(111) exhibits no fluence dependence at low primary ion dose. Using secondary neutral mass spectrometry (SNMS), the sputtering yield of ruthenium was observed to decrease following ion bombardment by argon, xenon, and neon. High-detection-efficiency time-of-flight mass spectrometry was coupled with nonresonant laser ionization to allow real-time sputtering yield measurements and to minimize target damage during data collection. The experiments show that the sputtering yield of Ru(0001) decreases by 50%, following a primary ion fluence of less than 10^{16} ions/cm^2 for sputtering by either argon or neon ions and by 25%, following primary ion fluences of less than 10^{14} ions/cm^2 for sputtering by xenon. Data analysis, using a simple phenomenological model, indicates that the damage cross section responsible for the decrease in the sputtering yield is quite small. The small size of the experimentally determined damage cross section suggests that microscopic changes in the surface structure cause the observed sputtering yield depression. In contrast to the ruthenium results, the sputtering yield of Al(111) appears to be insensitive to primary ion fluence at low fluences. Calculations using the TRansport of Ions in Matter (TRIM) Monte Carlo sputtering simulation were carried out to investigate the effect of primary ion implantation upon the sputtering yield of ruthenium as well as the effect of a reduced surface binding energy of ruthenium surface atoms. The TRIM results indicate that neither of these mechanisms can explain the experimentally observed fluence dependence of the sputtering yield of ruthenium.

1.1 Introduction

While it has been recognized that the sputtering yield of a material may be strongly influenced by surface topography and stoichiometry, it has generally been assumed that sputtering yields from clean metal surfaces are insensitive to ion bombardment at low-to-moderate fluences.[1] Ion dose effects upon the sputtering yield have previously been observed following high fluence bombardment. These changes in the sputtering yield following ion bombardment of the surface have generally been attributed to gross changes in the surface topography, such as cone formation, faceting, and surface roughening.[2-13] Typically, sputtering yields increase with surface roughness, whether caused by extensive ion bombardment or mechanical roughening.[2-10, 12] A few instances have been reported where specially prepared surfaces with steep cones resulted in decreaseed sputtering yields.[11, 13] Other workers who have observed an ion fluence dependence of the sputtering yield have determined that the sputtering yield was found to increase following the sputter removal of surface impurities.[6, 14-19] The sputtering yields from targets with surface contamination, such as carbon or oxygen, invariably were observed to increase following sputter removal of the surface contamination.[6, 16-19] In sputtering yield measurements from thin gold films grown onto a quartz crystal microbalance, Oliva Florio et al. observed a 20% decrease in the sputtering yield following an ion fluence of 10^{14} ions/cm^2, using 5 keV Ar^+.[20] This decrease in the sputtering yield was ascribed to the sputter removal of a surface layer of

loosely bound gold atoms. No explanation for the existence of a layer of loosely bound gold atoms was offered nor was experimental evidence for its existence presented. More recently, the self-sputtering yields from condensed rare gas solids have been observed to decrease dramatically following primary ion bombardment.[21-25]

Here we report on an investigation of the sputtering yield of an atomically clean Ru(0001) surface following ion bombardment using Ne, Ar, and Xe. As described in the text below, we have found that the sputtering yield decreases by as much as 50% following primary ion fluences of less than 10^{16} ions/cm^2. Similar experiments investigating the ion fluence dependence of the sputtering yield of an atomically clean Al(111) surface show no ion dose dependence.

1.2 Experimental

Experiments were carried out in a stainless steel UHV chamber pumped by a cryopump that attained a base pressure of 3 x 10^{-11} Torr following system bakeout. In addition to the SNMS apparatus, the chamber is equipped with an Auger spectrometer for surface characterization and a quadrupole mass spectrometer for residual gas analysis.

1.2.1 Nonresonant Ionization of Sputtered Neutrals

The sputtering yields of Ru(0001) and Al(111) were measured using multiphoton nonresonant laser ionization followed by mass spectrometric detection, a particular method of carrying out

SNMS. The SNMS apparatus may be partitioned into three subunits - the ion source, the ionizing laser, and the Energy and Angular Refocusing Time-of-Flight (EAR-TOF) mass spectrometer. A schematic diagram of the apparatus is provided in Fig. 1.

The primary ion beam was generated by a Colutron ion source which was both differentially pumped and mass analyzed. A 3.6 keV primary ion beam (argon, neon, or xenon) of 1-2 μA was produced by the source. An aperture was used to reduce the average ion current to 10-20 nA, and the ion beam was focused into a 200 μm diameter spot on the target. The primary ion beam was used for both controlled ion bombardment (damage) of the surface and for the actual sputtering yield measurements. The target was damaged by rastering the primary ion beam over a 1 mm^2 area of the target for a known amount of time. The size of the rastered area on the target was chosen to assure that a large area of the target was uniformly damaged. During data collection, the ion beam was directed to the center of the damaged area and then temporally chopped into 500 ns pulses by deflection across an aperture. A Faraday cup was used to measure the dimensions of the ion beam and the rastered area and to align the primary ion beam to the center of the rastered area.

The second subunit of the SNMS apparatus is the laser. The output from a XeCl excimer laser (Lambda Physik model EMG 201 MSC), which produces light with a 3 - 5 Å bandwidth at 3079 Å (4.03 eV), was used for the nonresonant ionization of sputtered species from the Ru(0001) target. The ionization of the ruthenium atom with an ionization potential of 7.36 eV requires

two 3079 Å photons. The ionization of sputtered neutral species from the Al(111) target was performed using an ArF excimer laser (Questek model 2860) which generates light with a wavelength of 1930 Å (6.42 eV) and a spectral bandwidth of approximately 3-5 Å. Because of the low ionization potential of an Al atom, 5.99 eV, relative to the energy of an 1930 Å photon, the ionization of Al was a single photon process. The typical laser pulse energy used for the Al(111) and Ru(0001) experiments was 1-5 mJ delivered into a 1 mm x 3 mm rectangular laser spot, corresponding to a power density of 3-15 MW/cm^2. The laser was oriented such that the 3 mm side of the rectangular laser spot was parallel to the target surface and was positioned as close to the target surface as possible in order to maximize the solid angle of collection.

The final section of the apparatus is the EAR-TOF mass spectrometer. As an aid in understanding the operation of the instrument, the reader is referred to the schematic diagram Fig. 1 and the timing diagram that is shown in Fig. 2. A data collection cycle begins with the creation of the ion pulse. To accomplish this, the primary beam is swept across an aperture by a set of pulsed deflection plates. The ion pulse traverses an electrostatic lens and an additional set of deflection plates before passing through the primary ion turning plates that merge the primary ions onto the EAR-TOF axis by means of electrostatic deflection. As can be seen in Fig. 2, the primary ion pulse strikes the target normal to the surface during a time when the sample is held at 1350 V (nominal). This target potential results in the production of secondary ions with an energy of

1350 eV. Once the entire ion beam has reached the target, the target potential is lowered to approximately 1100 V and the excimer laser is fired. Photoions with an energy of 1000 eV are generated in a spatial region that extends from approximately 0.5 to 1.0 mm above the target surface. The photoions traverse the additional lens and are focused through the primary ion beam turning plates which have been lowered to 0 V as shown in Fig. 2. Following a flight path of 80 cm, the photoions are focussed into the first of two resistive disk energy analyzers. These two resistive disk energy analyzers are spherical energy analyzers that have been designed to have a large angular and energy acceptance. The energy analyzers allow ions with energies of 900 - 1100 eV to pass through them. Secondary ions are discriminated against since they were extracted with 1350 V. Photoions, on the other hand, are extracted with 1000 V and are therefore transmitted through the energy analyzers. Following traversal of the two spherical energy analyzers, the ions strike a pair of chevron microchannel plates. They are then detected by a gated pulse counting system.

The high-detection efficiency of this technique allowed sputtering yield data to be obtained under static conditions, using less than 3×10^{11} primary ions/cm^2 per data point. Each data point was the result of 800 averages and yielded a signal-to-noise ratio > 60. The low fluences used for data collection in these experiments correspond to less than one ion impact for every 5300 surface atoms, a fluence low enough to assure that ion beam damage does not influence measurements. To confirm this

fact, the SNMS signal was monitored for much lower fluences, $< 10^{10}$ primary ions/cm^2. No change in sputtered particle signal levels was observable for these very low fluences.

Because the neutral atomic species are generally > 90% of the sputtered flux from clean metal surfaces, measurements of neutral atom yields closely approximate measurements of the actual sputtering yield.[26-28] Care has been taken to assure that the experiments are insensitive to variations in both the angular and velocity distribution of the sputtered species. The experiments were designed to utilize a relatively large laser ionization volume in order to maximize the solid angle of collection. This coupling of a large ionizing laser volume relative to the ion spot size results in a solid collection angle of > 2.8 sr. Assuming a cosine distribution[29] of sputtered atoms, approximately 70% of the ejected atoms pass through the laser ionization volume; therefore, the results presented here are believed to be independent of any changes in the sputtered atom angular distribution. To assure that a significant fraction of the sputtered atom energy distribution intersects the laser volume at the time the lasers are fired, a relatively long ion pulse width (800-1000 nsec) has been employed. Experiments indicate that no increase in the signal level occurs for ion pulse widths greater than 400 ns. Thus, a steady-state neutral population in the laser ionization volume is believed to be reached at this ion pulse width. In addition, the signal levels for various segments of the sputtered atom energy distribution were measured by changing the time that the laser fires relative

to the time that the primary ion strikes the target. The results were observed to be independent of the sputtered atom energy distribution.

1.2.2 Experimental Methods Utilized in Sputtering Yield Measurements

For these experiments, the SNMS signal from a sputtered portion of the Ru(0001) surface was repeatedly compared with the signal from the undamaged portion of the surface. Thus each sputtering yield measurement involved measuring the sputtering yield from both the ion bombarded and the unsputtered portions of the crystal. Typically, data were collected from two positions on the crystal face. The ion beam was first centered on one of these positions and the Ru sputtered flux was measured. The crystal was then translated 3-4 mm to the second position and sputtering data were again collected. This translation between the two positions and data collection was repeated 4-5 times thereby removing any effects caused by fluctuations in laser intensity or in the instrument transmission. One of the positions then received a carefully controlled dose of primary ions. Following the ion bombardment, data were again repeatedly collected from the damaged and the undamaged portions of the target. By continuing this process of data collection and ion bombardment, primary ion fluences of $> 10^{16}$ ions/cm^2 were accumulated in the ion bombarded portion of the target.

To minimize the time that the crystal was exposed to residual gases, a second series of experiments was carried out

using a much higher primary ion current (200 nA) ion beam. In these experiments, which were conducted for Ar^+ bombardment, the primary ion dose was not accumulated over a long period of time; rather, the crystal was bombarded continuously (for 3 minutes) until a fluence of $> 10^{16}$ ions/cm^2 was attained. These data ascertained that the observed Ru(0001) sputtering yield, following a primary ion fluence of $> 10^{16}$ ions/cm^2, was identical regardless of whether the crystal was bombarded over a long or a short period of time.

Experiments were also carried out with the Ru(0001) crystal tilted at +10° and -10° relative to the primary ion beam in order to observe the dependence of the sputtering yield on the primary ion angle of incidence. For these experiments, the primary ion beam current was 200 nA and the rastered beam size was 2 mm^2.

1.2.3 Ru(0001) Crystal Preparation

The Ru single crystal, purchased as a 99.97% pure boule oriented along the (0001) axis from Metal Crystals and Oxides, LTD, was cut and oriented along the (0001) axis to within ± 1° using Laué back reflection and polished to a mirror finish. A chromel-alumel thermocouple was press-fitted into the edge of the crystal for temperature measurement. Two grooves were cut into the edges of the crystal by spark erosion in order to support the crystal on tungsten leads. The crystal was supported in front of a tungsten filament which was used for either radiative or electron bombardment heating of the target. The crystal was cleaned by repeated heating to 1450 K in 10^{-6} Torr of oxygen

followed by heating to 1550 K in vacuum.[30-37] Auger electron spectroscopy (AES), SNMS and SIMS analyses were used to monitor surface cleanliness and to confirm that no impurities were introduced to the surface by the primary ion beam. Because of the overlap between the carbon Auger feature near 274 eV and the Ru 274 eV feature, carbon contamination is difficult to quantify. Minimizing the (-/+) Auger signal ratio at 274 eV has been assumed to indicate a carbon-free surface by many researchers.[30-37] The reported limiting value of (-/+) Auger signal ratio at 274 eV is 1.20.[30-32, 35] Examination of a heavily carbon-contaminated Ru(0001) surface has revealed that SNMS ruthenium carbide signal levels are correlated with carbon contamination and that this is a much more sensitive indicator of carbon contamination than is the (-/+) Auger ratio method.[38] A Ru(0001) crystal, judged to be clean, exhibited a (+/-) Auger ratio of 1.21 ± .02. In the experiments reported here, the surface carbon concentration was always < 5 at.% as determined by SNMS. Auger and SNMS analyses ascertained that no other surface contaminants were present.

Following heavy ion bombardment of the Ru crystal, Auger, SIMS, and SNMS analyses were used to confirm that no contamination was introduced to the target by the primary ion beam. The base pressure in the UHV chamber was 2.7×10^{-11} Torr and increased to $5\text{-}9 \times 10^{-10}$ Torr during sputtering. A quadrupole mass spectrometer revealed that the gas used for sputtering was the major residual gas responsible for the

pressure rise during sputtering, accounting for ~ 80% of the gas composition.

1.2.4 Al(111) Crystal Preparation

The Al(111) crystal used in these experiments was cut from a 99.999% pure boule purchased from Materials by Metron. The boule was oriented to within 2° of the (111) axis using Laue back reflection and then cut by spark erosion into a 1-2 mm thick slice. The Al slice was then reoriented along the (111) axis to ±0.5° and polished to a mirror-finish. The Al(111) target was mounted onto a heater button (Spectra Mat., Inc.) and held in place by a tantalum cup. Using the heater button, the target could be heated to temperatures in excess of 700 K. Extensive cycles of sputtering with 1.5 keV Ar^+ and annealing at 700 K were required to remove surface carbon presumably introduced during the polishing process. AES was used to monitor target cleanliness. During the initial sputtering and annealing cycles, the target lost its mirror-finish and appears dull white (matte finish) as was observed previously by other workers.[39, 40] Low energy electron diffraction studies[40] show that the Al(111) surface following the cleaning procedure results in a sharp (1x1) diffraction pattern indicating a well-ordered surface despite the matte finish.

Once the initial carbon impurities were removed, the daily cleaning procedure consisted of sputtering the crystal for 45 minutes at 300 K, followed by 45 minutes of sputtering with the crystal held at 700 K. To anneal the crystal, the Al(111) target

was held at 700 K for 15 minutes. AES results indicated that carbon and oxygen impurity levels were < 1 at.% following the cleaning procedure.

2 The sputtering yield from Ru(0001) as a function of primary ion fluence following bombardment by Ne^+, Ar^+, and Xe^+

In Fig. 3, the experimental results for Ru(0001) are displayed. The sputtering yield from the ion damaged surface is referenced to that from the undamaged surface and plotted as a function of primary ion fluence. The sputtering yield from the ion bombarded region of the target was repeatedly compared to that from the undamaged portion of the target during each yield measurement for a particular primary ion fluence to determine the reproducibility of the measurement. Each point displayed in Fig. 3 is the result of the average of several (3-4) different experimental runs. Figs. 3(a), (b), and (c) are the experimental results using different primary ions, Ne^+, Ar^+, and Xe^+, respectively. The solid curve in each plot is the result of a least squares fit of the data to a phenomological model which is described below. For all three different primary ions: (1) the sputtering yield is observed to decrease substantially and (2) the decrease saturates at some primary ion fluence. Bombardment by Ne^+ and Ar^+ results in a two-fold reduction in the sputtering yield of Ru(0001) while bombardment by Xe^+ results in a 25% decrease in the sputtering yield. The depression in the sputtering yield caused by Xe^+ bombardment saturates at

relatively low primary fluences, specifically at 4×10^{14} ion/cm^2, when compared to Ar^+ or Ne^+ which saturate at 2×10^{15} and 8×10^{15} ions/cm^2, respectively.

If the sputtering yield depression is associated with damage to the Ru(0001) surface, the primary ion fluence required to reach saturation of the sputtering yield may be considered in terms of the damage associated with the particular ion involved. Xe^+, a massive ion, deposits most of its energy nearer to the surface than either Ar^+ or Ne^+. Ne^+, the smallest primary ion used for these experiments, penetrates the target most deeply, depositing less of its energy at the surface. For a fixed primary ion energy, Xe^+ bombardment of the Ru surface results in a higher sputtering yield, followed by Ar^+ bombardment, and Ne^+ bombardment. Therefore, surface damage per incident ion is greatest for bombardment by Xe and least for Ne bombardment. It is reasonable, then, that Xe^+ bombardment leads to saturation of the sputtering yield earliest in terms of ion fluence for the three primary ions employed. In line with this reasoning, the decrease in the sputtering yield is observed to saturate following Ar^+ bombardment at fluences intermediate to those following bombardment by Xe^+ and Ne^+.

2.1 Phenomenological Model

At low ion fluences, where the decrease in the sputtering yield has not yet saturated, only a fraction of the bombarded portion of the Ru crystal has been damaged by a primary ion impact. In this ion fluence range, the Ru SNMS signal, I_{OBS}, from

the sputtered portion of the crystal can be partitioned into two distinct contributions. The first is the total signal arising from ion impacts of undamaged sites, I_0, and the second is signal arising from previously bombarded sites, I_{DAM}. The relative contribution from each of these is dependent upon the accumulated primary ion fluence, J:

$$I_{OBS}(J) = I_{DAM}(J) + I_0(J) \qquad (1)$$

The signal arising from each of these sites is proportional to the number of the respective sites available. At very low fluences, very little of the target surface has been damaged and the SNMS signal is dominated by Ru atoms ejected from undamaged sites. At moderate fluences, both damaged and undamaged sites contribute to the SNMS signal. At very high fluences, the entire crystal surface has been impacted at least one time, and all of the observed signal arises from damaged sites. Using Poisson statistics and defining a damage cross section, σ, for a single ion impact as *the area responsible for the reduction in sputtering yield*, then:

$$I_{DAM} = \xi\, Y_{DAM} \left(1 - e^{\left(-\sigma J\right)}\right) \qquad (2)$$

and

$$I_0 = \zeta Y_0 \, e^{(-\sigma J)} \qquad (3)$$

The detection efficiency for Ru in our instrument is ζ: Y_0 and Y_{DAM} are the sputtering yields from previously impacted and undamaged sites, respectively. The fraction of the surface, which has been impacted at least once, is $1 - e^{(-\sigma J)}$ so that $e^{(-\sigma J)}$ is the fraction of the virgin surface remaining. Combining Eqs. 1-3 yields:

$$\left(\frac{I_{OBS}\,(J)}{I_{OBS}\,(J=0)} \right) = \frac{Y_{DAM}}{Y_0} + e^{(-\sigma J)} \left(1 - \frac{Y_{DAM}}{Y_0} \right) \qquad (4)$$

Since the observed signal from the sputtered portion of the crystal is $I_{OBS}(J)$, the signal from the unsputtered area is $I_{OBS}(J=0)$. The data was fit to the model allowing the damage cross section, σ, and the ratio of the damaged to undamaged sputtering yields, Y_{DAM}/Y_0, to be adjustable parameters. As Fig. 3 shows, the agreement between the experimental results and the model is excellent for all the primary ions used.

A summary of the experimental and model results are presented in Table 1. For comparison, the sputtering yields of ruthenium are included in this table. The damage cross section is observed to increase with increasing sputtering yield. Fig. 4a shows that the number of surface Ru atoms contained within the damage cross section increases with, but also more rapidly than, the sputtering yield. In Fig. 4b, it is apparent that the number

of atoms contained in the damage cross section increases linearly with the square of the sputtering yield. The cause of this rapid increase in the size of the damage cross section is not clear. Bombardment by Ne^+ and Ar^+ result in similar sputtering yield depressions, Y_{DAM}/Y_O, at the high ion fluence limit whereas Xe^+ bombardment causes a smaller depression in the sputtering yield.

Several factors must be considered in assessing the meaning of these results. The first concerns the nature of the damage to the Ru(0001) surface. Closely related to this question is the cause of the sputtering yield depression, that is, whether it is the primary particle interaction with a damaged surface, or whether it is the recoil trajectory from a damaged target that is primarily responsible for the observed behavior. One would expect that, if the effect were due principally to changes in recoil atom escape trajectories and if the surface damage caused by the different primary ions were similar, the yield suppression would be identical for the three primary ions studied. The fact that they are different indicates two possibilities. The first is that the damage induced by the different ions is different. The second is that the primary ion energy loss in the damaged target is different from that in the undamaged target.

The decrease in the sputtering yield of Ru following low fluence ion bombardment was a surprising and unexpected result. Because of this, various tests were carried out to investigate whether indeed a significant physical phenomenon had been observed.

3. Investigations of Surface Impurities

It is conceivable that a surface impurity could lead to an enhanced sputtering yield. If an adsorbed impurity significantly reduced the binding energy of the Ru atoms in the near-surface region by forming strong chemical bonds, the sputtering yield of the Ru could increase. Sputter removal of the contaminant would then lead to a decrease in the Ru sputtering yield. Two different experiments were carried out to ascertain that the observed sputtering yield depression was not caused by the presence of impurities.

Because of the overlap of the Ru and carbon (C) Auger features as discussed earlier, the most probable surface contaminant would be carbon. Surface contamination by other common impurities such as oxygen or sulphur is unlikely as they are easily detected by SIMS, AES, or SNMS. The sputtering experiment was carried out on a heavily C-contaminated surface[38] to help rule out the possibility that our results were due to the presence of a surface carbide. The results of this experiment are shown in Fig. 5 where the Ru signal following ion bombardment [I(J)] is again referenced to the Ru signal from an undamaged, albeit contaminated, surface [I(J=0)]. Ar^+ was used as the primary ion for these experiments. The initial Ru signal is seen to decrease with ion dose quite similarly to that from a clean Ru surface. The magnitude of the decrease, however, is significantly less than that of the clean surface. However for the C-contaminated surface, the Ru signal is observed to pass through a minimum before reaching a steady-state signal level.

This is most likely due to two independent mechanisms. The first is the subject of this paper, namely, the reduction of sputtering yield due to ion-bombardment-induced damage. The second is the presence of a C overlayer which reduces the sputtering yield of the ruthenium, because sputtered atoms are known to originate predominantly from the outermost atomic layer.[41-45] In addition, the concentration of Ru in the near-surface region of the target is simply reduced by the presence of C. Once the C impurity has been sputtered away, Ru is the sole constituent and its sputtering yield increases. The SNMS Ruthenium carbide (RuC) signal, also plotted in Fig. 5, supports this explanation. The maximum RuC signal is expected to occur when the Ru and C concentrations are equal. The peak of the RuC signal occurs at the very minimum of the Ru signal ratio, presumably because of an equal concentration of Ru and C. The RuC signal is observed to decrease with increasing ion dose, as expected since sputtering removes the carbon from the Ru. Based on the assumption that the maximum RuC concentration occurs at equal C and Ru concentrations, and further assuming that the RuC signal is linearly related to the C concentration, the atomic fraction of C can be calculated from the RuC signal levels. Assuming also that the limiting, high-ion-dose sputtering yields are equal for both the clean and the carbon-contaminated Ru surfaces, these results indicate that the presence of C reduces the initial, undamaged Ru sputtering yield by ~25%. Furthermore, at ion fluences greater that 10^{15} Ar^{+}/cm^{2} where the C concentration is decreasing, the Ru signal is observed to increase. Thus, the presence of a surface

C impurity that sputters away cannot be an explanation for the ion-dose dependent decrease in the Ru sputtering yield shown in Fig. 3.

3.1 Investigations of the effect of primary ion flux

An additional series of experiments investigated the possibility that the residual gas in the UHV chamber was a source of surface contamination. Experiments were carried out which minimized the data collection time, thereby reducing the possibility of adsorption of residual gases. In these experiments, the primary ion beam current was increased to 200 nA, reducing the time required to reach the saturated sputtering yield depression. Ar^+ was again used as the primary ion. The clean crystal was quickly heated before data collection and ion bombardment to remove any adsorbed gases. Data was collected only from the undamaged crystal and following heavy ion bombardment at fluences greater than 10^{16} Ar^+/cm^2. These experiments reproducibly showed a 50% reduction in the Ru sputtering yield following ion bombardment. Furthermore, annealing the crystal to 1500 K after ion bombardment returned the sputtering yield of the damaged surface to its original, undamaged level. These experiments confirmed that an impurity is not causing the observed ion dose dependence of the sputtering yield of Ru(0001) and that the sputtering yield decrease observed at high ion fluences is independent of the primary ion flux utilized.

3.2 The effect of changing the primary ion angle of incidence

At the low primary ion energies used in these experiments, channeling is not expected to play a significant role in the sputtering process. Furthermore, it is expected that ion-induced damage to the Ru single crystal would in fact result in the reduction of crystallinity, as in the creation of interstitial atoms and amorphization of the crystal surface. Such radiation damage is known to reduce the channeled fraction of the incident particles by effectively closing some fraction of the channels and therefore causing an increase in the sputtering yield.[46]

To determine the possible influence of ion bombardment along channeling directions, experiments were carried out using an Ar^+ beam directed + 10° and - 10° away from the surface normal. We observed the identical sputtering yield depression at these angles as at normal incidence. While this angle of ion bombardment is still near the axial channeling direction, these results suggest that the sputtering yield depression is not strongly coupled to the crystal structure. Since the experiments clearly show a decrease in the sputtering yield following ion bombardment, it is not possible for channeling to be responsible for the experimental results.

4 The sputtering yield of Ru(0001) at high temperature following high-dose primary ion bombardment

An experiment was carried out to observe the effect upon the sputtering yield following high primary ion fluences while

holding the ruthenium target at an elevated temperature. For these experiments, the sputtering yield was measured, following high primary ion fluences only, at fluences > 10^{17} Ar^+/cm^2. The signal from the damaged portion of the crystal was repeatedly compared with that from the undamaged portion of the crystal. The target was held at a temperature of 690 K during both the primary ion bombardment and the data collection. A 200 nA Ar^+ beam was used for damaging the surface as well as for the sputtering yield measurements.

With the crystal held at 690 K, the sputtering yield of Ru(0001) from the damaged portion of the target was found to be identical to that from the undamaged portion of the target. These results suggest that the surface damage responsible for the sputtering yield reduction in the room temperature experiments is removed by annealing at this temperature, which corresponds to roughly 25% of the melting point. (The melting point of ruthenium is 2583 K.) While this may seem to be relatively low temperature for annealing (typically temperatures of 50% of the melting point are used for annealing ion-induced damage), Winograd et al. have observed what they call "ion-induced" healing. These workers have observed that the number of ion-induced surface defects, adatoms or vacancies, is strongly reduced if the target is held at some elevated temperature during energetic primary bombardment. The number of defects is much lower than if the primary ion bombardment of the crystal is performed with the target held at low temperatures and then brought to the elevated temperature. This indicates that,

because the target is at an elevated temperature during the collision cascade, a fraction of defect atoms in the cascade has sufficient energy to recrystallize.

5 The ion dose dependence of the sputtering yield of Al(111)

The effect of Ar^+ bombardment upon the sputtering from an Al(111) surface was investigated in the same manner as that of the Ru(0001) target. In these experiments, the sputtering yield from an undamaged Al(111) surface was compared to that from a heavily-bombarded surface. The sputtering yields from both the damaged and undamaged surfaces were identical, and no fluence dependence of the sputtering yield of Al(111) was observed. It should be noted that these experiments were carried out at ambient temperature, ~295 K, which for aluminum is approximately 30% of the melting point. (The melting point of aluminum is 933 K.) It may well be that, at ambient temperature, any surface damage that could result in a reduction in the sputtering yield is annealed in the case of aluminum.

It is instructive to compare the results of the Al(111) sputtering yield measurements with those of the Ru(0001) measurments. The observation that no change in the sputtering yield of Al(111) occurs following primary ion bombardment strongly suggests that primary ion implantation is not responsible for the sputtering yield reduction observed in the Ru(0001) experiments.

6 TRIM calculations

In order to gain some insight into the experimental observation of a decrease in the sputtering yield of Ru(0001) following moderate ion fluences, calculations using the TRansport of Ions in Matter (TRIM) computer code[47-50] were performed. The TRIM code is a binary collision Monte Carlo sputtering code that models energetic ion bombardment of amorphous targets. TRIM calculations were carried out to determine whether the implantation of the primary ion could result in the decrease in the sputtering yield of Ru, and if so, to determine the magnitude of the decrease. In addition, calculations were carried out to investigate how a reduced surface binding energy in the outermost Ru layers would enhance the sputtering yield of the Ru. This second calculation models a Ru target which has a reduced surface binding energy before any ion bombardment has occurred.

6.1 TRIM calculation of the Effect of Implanted Primary Ions upon the Sputtering Yield of Ru

For the clarity of the discussion, the TRIM calculations of the effect of implanted primary ions can be broken into several portions. The first calculations carried out were to determine the implantation profiles of the primary ions. For these calculations, 3.6 keV primary ions impinged an amorphous ruthenium target and the probability that they were implanted at a given depth was determined. The results of these calculations are shown in Fig. 6, where the fractional concentration of the

implanted primary particles, that is, the number of primary particles per substrate atom, is plotted as a function of depth. The total primary ion fluence used for these calculations was chosen to be the fluence at which the sputtering yield suppression saturates in the experimental measurements. These values are displayed in each of the plots in Fig. 6.

Once the implantation profiles of the primary ions were determined, the sputtering yield of the implanted model target was calculated. In Fig. 7, the model implanted targets are shown. Because the TRIM code allows only three regions in the target with different stoichiometries, the depth distribution of the implanted target is a histogram. For each of the three different stoichiometries of the target, the concentration of the primary ion was chosen as the maximum concentration determined from the implantation profile calculation, Fig. 6. This is a limiting concentration; the true concentration in the implanted region is expected to be lower. This is especially true in the near-surface region where no implanted primary particles are expected to remain because they are not bound to the substrate. Two different implantation models were used. The first was a substitutional implant, that is, the implanted primaries were substituted for ruthenium atoms. The number density of the ruthenium atoms in the target was therefore reduced by primary implantation. The second implantation scheme used was interstitial implantation, that is, the number density of the ruthenium atoms in the target remained unchanged when primary particles were incorporated into the target.

The primary-implanted targets model the ion-bombarded target of the experiment. The sputtering yield of the implanted targets are compared with the sputtering yield from a pure ruthenium target, and is shown in Fig. 8. The sputtering yield of the implanted ruthenium target is referenced to the sputtering yield from pure ruthenium. The experimental sputtering yield ratio is also shown for comparison. The experimental sputtering yield ratio is the high-ion fluence limit of the sputtering yield measured on the ion-damaged surface referenced to the yield measured on the undamaged surface.

While it is clear that the implantation of the primary ions is unable to account for the reduction in the sputtering yield observed in the experiment, the sputtering yield of the model ruthenium targets is decreased slightly due to the implantation of primary particles. The decrease in the sputtering yield following primary implantation as determined by the TRIM calculation is observed to be greatest for neon implantation and least for xenon. This reflects the fact that the fractional concentration of the neon in the model ruthenium target was greatest and that of xenon least.

6.2 TRIM calculation of the Effect of a Reduced Surface Binding Energy for an Undamaged Surface.

The TRIM code was also used to determine whether a decreased surface binding energy for the first and/or second monolayer of the ruthenium would show an enhanced sputtering yield. The idea is that first and/or second monolayer ruthenium atoms are loosely

bound relative to the bulk ruthenium atoms and that they are removed by sputtering in the course of the ion fluence experiment. This mechanism would show an initially high sputtering yield and as the loosely bound atoms are removed, the sputtering yield would decrease and eventually reach a constant value representative of the bulk binding energy. Fig. 9 shows schematically the approach taken in the TRIM calculations. Calculations were performed on two different model ruthenium targets with a reduced surface binding energy. The first model target had a single monolayer of ruthenium atoms with a surface binding energy of 3.3 eV, which is approximately one-half of the sublimation energies. The second model investigated had two monolayers with a reduced surface binding energy. The sputtering yields calculated on these model targets were compared with the sputtering yield calculated from a target with a single surface-binding energy, 6.7 eV, corresponding to the heat of sublimation of ruthenium.

The results of these calculations are displayed in Fig. 10. In this case, the sputtering yield of the target with one or two monolayers having a reduced surface binding energy are referenced to the ruthenium target with a single surface binding energy. Again, the experimentally determined sputtering yield ratios are plotted for comparison. While these results indicate that a surface layer of loosely bound ruthenium atoms can result in a significant decrease in the sputtering yield of ruthenium, the magnitude of the decrease is still quite low when compared with the experiment. Furthermore, it is apparent that the decrease in

the yield is similar for all three of the primary species investigated. This is in contrast to the experimental results which clearly indicate that the yield depression is much smaller following xenon bombardment than bombardment by either neon or xenon.

7 Discussion

We have carried out studies of the sputtering yield of a carefully prepared ruthenium single-crystal target as a function of primary ion fluence. Experimental results show a significant decrease in the sputtering yield at moderate ion fluences. Data analysis indicates that a single ion impact is responsible for the sputtering yield depression. Moreover, the small size of the damage cross section suggests that surface vacancies or microroughness such as craters are responsible for the observed sputtering yield depression from an ion-damaged surface. It is clear that the damage cross section is much smaller in size than the two-dimensional projection of the entire collision cascade at the surface. Results from TRIM calculations show that (for sputtering by 3.6 keV Ar^+) sputtered atoms arise from the surface an average distance of 12 Å from the primary ion point of impact, the average surface area giving rise to sputtered atoms is 4.52×10^{-14} cm^2.

Experiments have been carried out using a deliberately contaminated ruthenium target, the results of which indicate that the sputtering yield depression is not caused by the presence of a surface C contamination. Using primary ions of different

masses results in a full 50% reduction in the sputtering yield following bombardment by argon and neon, while xenon bombardment results in a 25% reduction of the sputtering yield.

These differences in the magnitude of the sputtering yield depression strongly suggest that changes in the surface binding energies following bombardment are not responsible for the yield depression. If there existed one or two monolayers of loosely bound ruthenium atoms, the yield reduction would be expected to be similar for all three primary ions studied. TRIM calculations have been carried out which confirm that loosely bound surface atoms would lead to similar sputtering yield reductions for the three primaries used. The observation that the sputtering of Al(111) by Ar^+ shows no primary ion fluence dependence suggests that primary ion implantation is not responsible for the observed decrease in the sputtering yield of Ru(0001) following ion bombardment. TRIM calculations have also been used to test whether implantation of primary ions in the Ru target would lead to a sputtering yield decrease at high fluences. The results of these calculations show that the fluences used in the experiments are too low to account for the observed decrease in the sputtering yield. These results indicate that it is unlikely that surface contamination, primary ion implantation, or gross morphological changes are responsible for the observed ion fluence dependent decrease in the sputtering yield of Ru(0001).

In order to understand the cause of the observed decrease in the sputtering yield of Ru(0001) following low fluence ion

bombardment, consider the analytical formulation of the sputtering yield[29, 51]:

$$Y \alpha \frac{F_D(x=0)}{U_o} \qquad (5)$$

where $F_D(x=0)$ is the energy deposited in the near surface region and U_o is the surface binding energy. We have already determined that it is unlikely that a change in the surface binding energy is responsible for the observed decrease in the sputtering yield. It is possible that the ion bombardment of the target changes the energy deposition in the near-surface region. Two different ways of viewing this are possible. The first is that surface vacancies or craters allow the primary ion to penetrate deeply into the target before a collision occurs. This would mean that more of the energy of the primary particles is deposited deeper inside of the target thereby reducing the energy transferred to the atoms that are located near the surface. This would result in a reduced sputtering yield. The magnitude of the decrease in the sputtering yield would be expected to depend strongly upon the physics of the interaction of the primary with surface defects. The second way of looking at a change in the energy deposition in the near-surface region is to consider the recoil trajectories, that is, the ejection of the sputtered particles. Species ejected from a vacancy or crater bottom may be unable to escape the surface and more likely to be recaptured as they move

through the target surface. This in turn would be expected to reduce the sputtering yield from an ion-damaged surface.

8 Conclusions

The sputtering yield of Ru(0001) decreases following moderate-fluence ion bombardment. Bombardment by Ne^+ and Ar^+ results in a full 50% reduction in the sputtering yield while Xe^+ bombardment results in a 30% reduction in the yield. In contrast, the sputtering yield of Al(111) was found to be insensitive to primary ion fluence for bombardment by Ar^+. Data analysis of the Ru(0001) sputtering experimental results reveals that a single ion impact is sufficient to modify the surface resultant in a decreased sputtering yield. The damage cross section, that is, the size of the area that is responsible for the decrease in the sputtering yield, is small relative to the cross-sectional dimension of the collision cascade and is observed to increase linearly with the square of the sputtering yield. The small size of the damage cross section suggests that surface vacancies or crater formation is the cause of the reduction in the sputtering yield from the ion-bombarded surface.

Experiments were carried out to determine whether surface contamination was responsible for the fluence dependence of the sputtering yield of Ru(0001) which indicates that the decrease in the sputtering yield following ion bombardment is not the result of surface contamination. By changing the primary ion angle of incidence and observing the sputtering yield of Ru(0001) at high

primary fluences, the possibility that the reduction in the sputtering yield was associated with channeling was ruled out.

No ion fluence dependence of the sputtering yield was observed when the ruthenium target was held at an elevated temperature (25% of the melting point). Measurements of the sputtering yield of Al(111) at ambient temperature (30% of the melting point of aluminum) also showed no ion fluence dependence. This is most likely due to increased target atom mobility during the collision cascade at these temperatures, which are high relative to the melting point.

The insensitivity of the sputtering yield of Al(111) to primary ion fluence indicates that primary ion implantation is not likely to cause the observed decrease in the sputtering yield of Ru(0001) from an ion bombarded surface.

Calculations were carried out using the TRIM computer simulation to investigate whether a reduced surface-binding energy for the first and second monolayer of the ruthenium target could lead to the experimentally observed reduction in the sputtering yield. These calculations indicate that a reduced surface binding energy can lead to a reduced sputtering yield once the loosely bound ruthenium atoms are removed via sputtering. However, the magnitude of the sputtering yield reduction in this case would be similar for all three of the primary ions investigated in agreement with the predictions of analytical theory. In addition, TRIM calculations were carried out to determine the effect of implanted primary species upon the sputtering yield of ruthenium at high ion fluences. The results

of these calculations show that very little change in the sputtering yield occurs at the fluences used in these experiments, too little to account for the experimentally observed decrease in the yields.

†Present address: Ames Laboratory/Iowa State University, Ames, IA 50010

Table 1

Summary of experimental and model results of the primary ion dose dependent sputtering yield measurements.

Primary ion	Sputtering Yield of Ru(0001)	Damage Cross Section (cm^2)	Atoms Contained in Damage Cross Section	$\frac{Y_{DAM}}{Y_O}$	% Reduction of Sputtering Yield of Ru(0001)
Neon	1.2	4.4×10^{-16} cm^2	0.7	0.47	50 %
Argon	2.7	2.7×10^{-15} cm^2	4.3	0.49	50 %
Xenon	~3.8	8.1×10^{-15} cm^2	12.8	0.73	25 %

1. H. H. Andersen, H. L. Bay; in Sputtering by Particle Bombardment I: Physical Sputtering of Single-Element Solids, R. Behrisch, Eds. (Springer-Verlag, Berlin, 1981), pp. 145.

2. H. H. Andersen, H. L. Bay, Radiat. Eff., 19 (1973) 257.

3. H. H. Andersen, H. L. Bay, J. Appl. Phys., (1974) 953.

4. H. H. Andersen, H. L. Bay, J. Appl. Phys., 46 (1975) 1919.

5. H. H. Andersen, H. L. Bay, J. Appl. Phys., 46 (1976) 2416.

6. R. Behrisch, J. Roth, J. Bohdansky, A. P. Martinelli, B. Schweer, D. Rusbüldt, E. Hintz, J. Nucl. Mater., 93&94 (1980) 645.

7. P. Blank, K. Wittmaack, J. Appl. Phys., 50 (1979) 1519.

8. J. Bohdansky, H. Lindner, E. Hechtl, A. P. Martinelli, J. Roth, Nucl. Intrum. Methods Phys. Res., Sect. B, B18 (1987) 509.

9. P. P. Davidse, L. T. Maissel, J. Appl. Phys., 37 (1966) 574.

10. E. P. EerNisse, Appl. Phys. Lett., 29 (1976)

11. G. K. Wehner, D. J. Hajicek, J. Appl. Phys., 44 (1971) 2093.

12. J. L. Whitton, W. O. Hofer, U. Littmark, M. Braun, B. Emmoth, Appl. Phys. Lett., 36 (1980) 531.

13. J. F. Ziegler, J. J. Cuomo, J. Roth, Appl. Phys. Lett., 30 (1977) 268.

14. H. H. Andersen, H. L. Bay, Radiat. Eff., 13 (1972) 67.

15. H. H. Andersen, Radiat. Eff., 19 (1973) 257.

16. H. L. Bay, B. Schweer, P. Bogen, E. Hintz, J. Nucl. Mater., 111&112 (1982) 732.

17. H. L. Bay, Nucl. Intrum. Methods Phys. Res., Sect. B, B18 (1987) 430.

18. W. O. Hofer, H. L. Bay, P. J. Martin, J. Nucl. Mater., 76&77 (1978) 156.

19. Y. Matsuda, Y. Yamamura, Y. Ueda, K. Uchino, K. Muraoka, M. Maeda, M. Akazaki, Jpn. J. Appl. Phys., 25 (1986) 8.

20. A. R. Oliva Florio, E. V. Alonso, R. A. Baragiola, J. Ferron, Radiat. Eff. Lett., 76 (1983) 137.

21. V. Balaji, D. E. David, T. F. Magnera, J. Michl, H. M. Urbassek, Nucl. Instrum. Methods Phys. Res., Sect. B, Accepted.

22. J. W. Boring, D. J. O'Shaughnessy, J. A. Phipps, Nucl. Instrum. Methods Phys. Res., Sect. B, B18 (1987) 613.

23. D. J. O'Shaughnessy, J. W. Boring, J. A. Phipps, R. E. Johnson, W. L. Brown, Nucl. Instrum. Methods Phys. Res., Sect. B, B13 (1984) 304.

24. D. J. O'Shaughnessy, J. W. Boring, J. A. Phipps, R. E. Johnson, Nucl. Instrum. Methods Phys. Res., Sect. B, B18 (1986) 304.

25. D. V. Stevanovic, D. A. Thompson, J. A. Davies, Nucl. Instrum. Methods Phys. Res., Sect. B, B1 (1984) 315.

26. M. J. Pellin, W. Husinski, W. F. Calaway, J. W. Burnett, E. L. Schweitzer, C. E. Young, B. Jørgensen, D. M. Gruen, J. Vac. Sci. Technol. B, 5 (1987) 1477.

27. F. M. Kimock, J. P. Baxter, N. Winograd, Surf. Sci., 124 (1983) L41.

28. A. Benninghoven, Surf. Sci., 53 (1975) 596.

29. P. Sigmund, Phys. Rev., 184 (1969) 383.

30. R. G. Musket, W. McLean, C. A. Colmenares, D. M. Makowiecki, W. J. Siekhaus, Appl. Surf. Sci., 10 (1982) 143.

31. J. E. Houston, C. H. F. Peden, D. S. Blair, D. W. Goodman, Surf. Sci., 167 (1986) 427.

32. D. W. Goodman, J. T. Yates Jr., C. H. F. Peden, Surf. Sci., 164 (1985) 417.

33. T. W. Orent, R. S. Hanson, Surf. Sci., 67 (1977) 325.

34. P. D. Reed, C. M. Comrie, R. M. Lambert, Surf. Sci., 59 (1976) 33.

35. H. Tochihara, G. Rocker, R. M. Martin, H. Metiu, J. T. Yates Jr., Surf. Sci., 203 (1988) 4.

36. K. Christmann, G. Ertl, H. Shimizu, J. Catal., 61 (1980) 397.

37. H. Shimizu, K. Christmann, G. Ertl, J. Catal., 61 (1980) 412.

38. J. W. Burnett, M. J. Pellin, W. F. Calaway, D. M. Gruen, J. T. Yates Jr., Phys. Rev. Lett., 63 (1989) 562.

39. J. E. Crowell, J. G. Chen, J. T. Yates Jr., Surf. Sci., 165 (1986) 37.

40. J. E. Whitten, C. E. Young, M. J. Pellin, D. M. Gruen, P. L. Jones, Surf. Sci.,

41. M. J. Pellin, J. W. Burnett, Pure Appl. Chem., Submitted

42. J. W. Burnett, J. P. Biersack, D. M. Gruen, B. Jørgensen, A. R. Krauss, M. J. Pellin, E. L. Schweitzer, J. T. Yates Jr., C. E. Young, J. Vac. Sci. Technol. A, 6 (1988) 2064.

43. B. Jørgensen, M. J. Pellin, C. E. Young, W. F. Calaway, E. L. Schweitzer, D. M. Gruen, J. W. Burnett, J. T. Yates Jr., in *Materials Modification by High-Fluence*

Ion Beams NATO Advanced Study Institute Viano do Castelo, Portugal, 1987), pp. in press.

44. K. M. Hubbard, R. A. Weller, D. L. Weathers, T. A. Tombrello, Nucl. Instrum. Methods Phys. Res., Sect. B, .

45. M. F. Dumke, T. A. Tombrello, R. A. Weller, R. M. Hously, E. H. Cirlin, Surf. Sci., 124 (1983) 407.

46. L. C. Feldman, J. W. Mayer; Fundamentals of Surface and Thin Film Analysis (North-Holland, New York, 1986).

47. J. P. Biersack, L. G. Haggmark, Nucl. Instrum. Methods Phys. Res., Sect. B, 174 (1980) 257.

48. J. P. Biersack, W. Eckstein, Appl. Phys., A34 (1983) 73.

49. J. P. Biersack, W. Eckstein, Appl. Phys., A34 (1984) 73.

50. J. P. Biersack, Nucl. Instrum. Methods Phys. Res., Sect. B, 27 (1987) 21.

51. P. Sigmund; in Sputtering by Particle Bombardment I: Physical Sputtering of Single-Element Solids, R. Behrisch, Eds. (Springer-Verlag, Berlin, 1981), pp. 9.

Figure 1 Schematic view of the EAR-TOF SNMS instrument.

Figure 2 Timing diagram of the SNMS experiments. See text for details.

Figure 3 The normalized sputtering yield of Ru(0001) is plotted as a function of primary ion fluence following bombardment by (a) Ne^+, (b) Ar^+, and (c) Xe^+. The sputtering yield from the damaged portion of the Ru(0001) crystal in each plot is refer enced to the sputtering yield from the undamaged surface. The smooth curve in each plot is the result of a simple phenomenological model which is fully described in the text.

Figure 4 (a) The number of atoms contained in the damage cross section, σ, are plotted as a function of the sputtering yield while in (b) the number of atoms contained in σ are plotted as a function of the square of the sputtering yield for each of the three primary ions. The curves drawn through the data points are to guide the eye.

Figure 5 The ratio of the Ru signal from a heavily carbon-contaminated, ion-damaged Ru surface to the Ru SNMS signal from an undamaged surface is plotted as a function of primary ion dose. For comparison, the RuC signal is also plotted. The solid line represents the calculated atomic fraction of carbon in the surface region.

Figure 6 TRIM calculation of the concentration of primary ions in the ruthenium target as a function of depth because of primary ion implantation.

Figure 7 The concentration profiles of the targets used in calculating the effect of primary ion implantation upon the sputtering yield of ruthenium with TRIM.

Figure 8 The experimental sputtering results are compared with the results of the TRIM calculation of the effect of primary ion implantation on the sputtering yield. The experimental sputtering yield ratio is the ratio of the sputtering yield from an undamaged surface referenced to that of the damaged surface. The calculated data points are the ratios of the sputtering yield from a target with no loosely bound atoms referenced to the yield from a target with one or two layers of loosely bound atoms.

Figure 9 Schematic diagram depicting the layer structures used for the TRIM calculations investigating the effect of a reduced surface binding energy upon the sputtering yield of ruthenium. (a) shows a ruthenium target with a single monolayer having a surface binding energy one-half that of the bulk crystal. (b) is a target with two layers having a reduced surface binding energy. These targets are intended to represent an undamaged target which has loosely bound surface atoms. The ion-damaged target in this model is shown in (c) and is characterized by a surface in which all of the loosely bound surface atoms have been removed by sputtering.

Figure 10 The experimental sputtering results are compared with the results of the TRIM calculation of the effect of a loosely bound surface layer of atoms on the sputtering yield. The experimental sputtering yield ratio is the ratio of the sputtering yield from an undamaged surface referenced to that of the damaged surface. The calculated data points are the ratios of the sputtering yield from a target with no loosely bound atoms referenced to the yield from a target with one or two layers of loosely bound atoms.

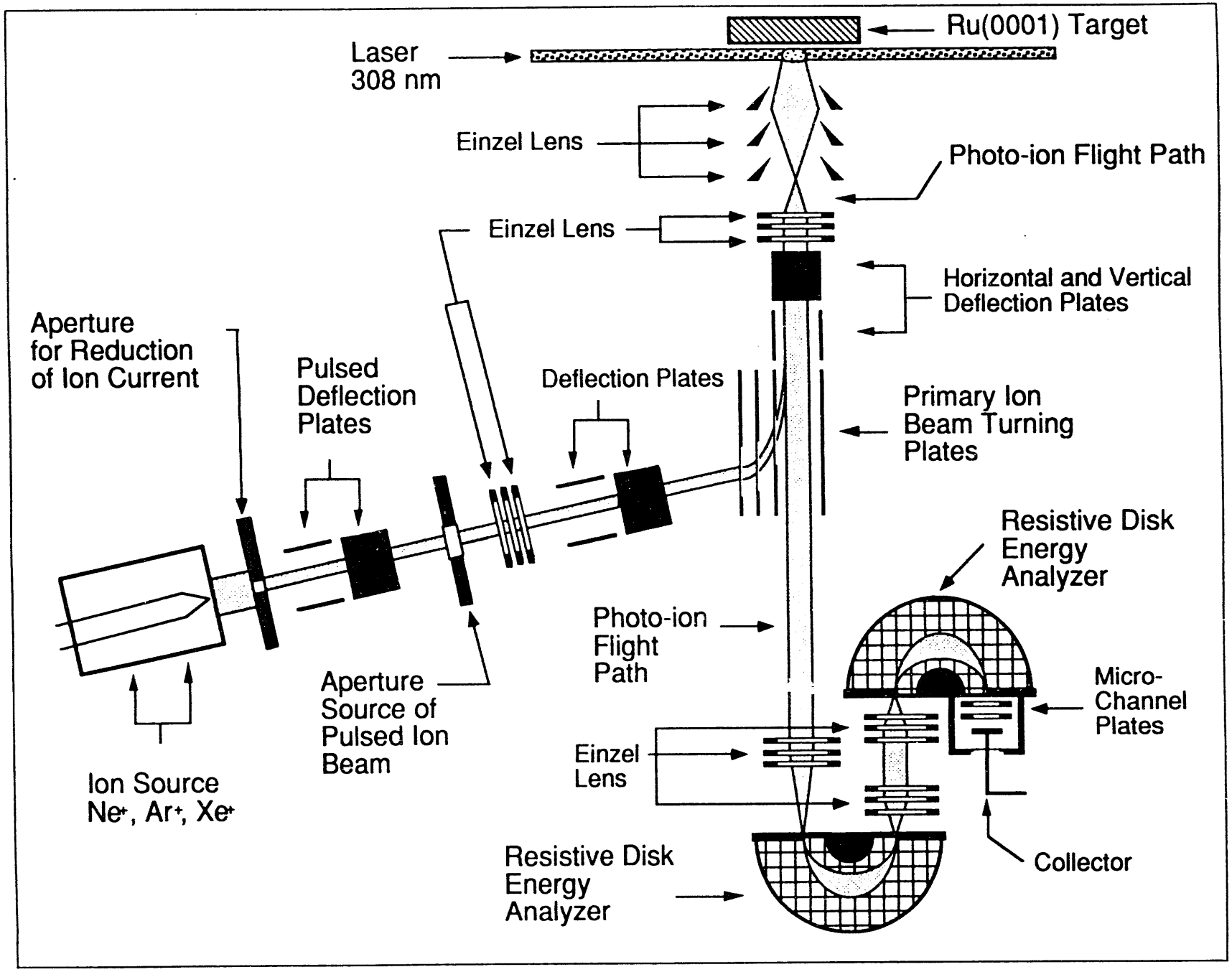
Ru(0001) Target
Laser
308 nm
Einzel Lens
Photo-ion Flight Path
Einzel Lens
Horizontal and Vertical
Deflection Plates
Aperture
for Reduction
of Ion Current
Pulsed
Deflection
Plates
Deflection Plates
Primary Ion
Beam Turning
Plates
Resistive Disk
Energy
Analyzer
Photo-ion
Flight
Path
Micro-
Channel
Plates
Aperture
Source of
Pulsed Ion
Beam
Einzel
Lens
Ion Source
Ne+, Ar+, Xe+
Resistive Disk
Energy
Analyzer
Collector

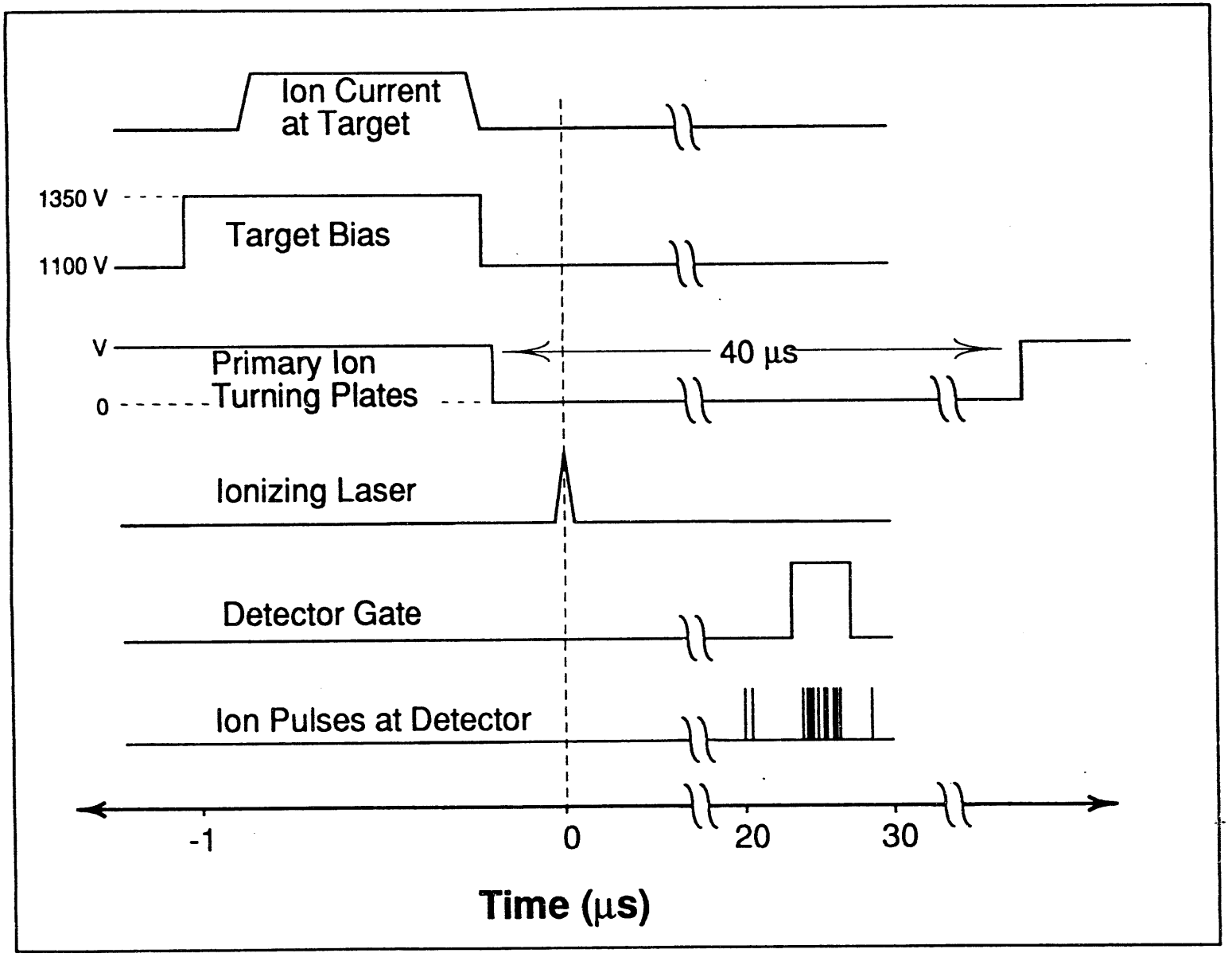
Ion Current
at Target
1350 V
1100 V
Target Bias
V
0
Primary Ion
Turning Plates
40 µs
Ionizing Laser
Detector Gate
Ion Pulses at Detector
-1
0
20
30
Time (µs)

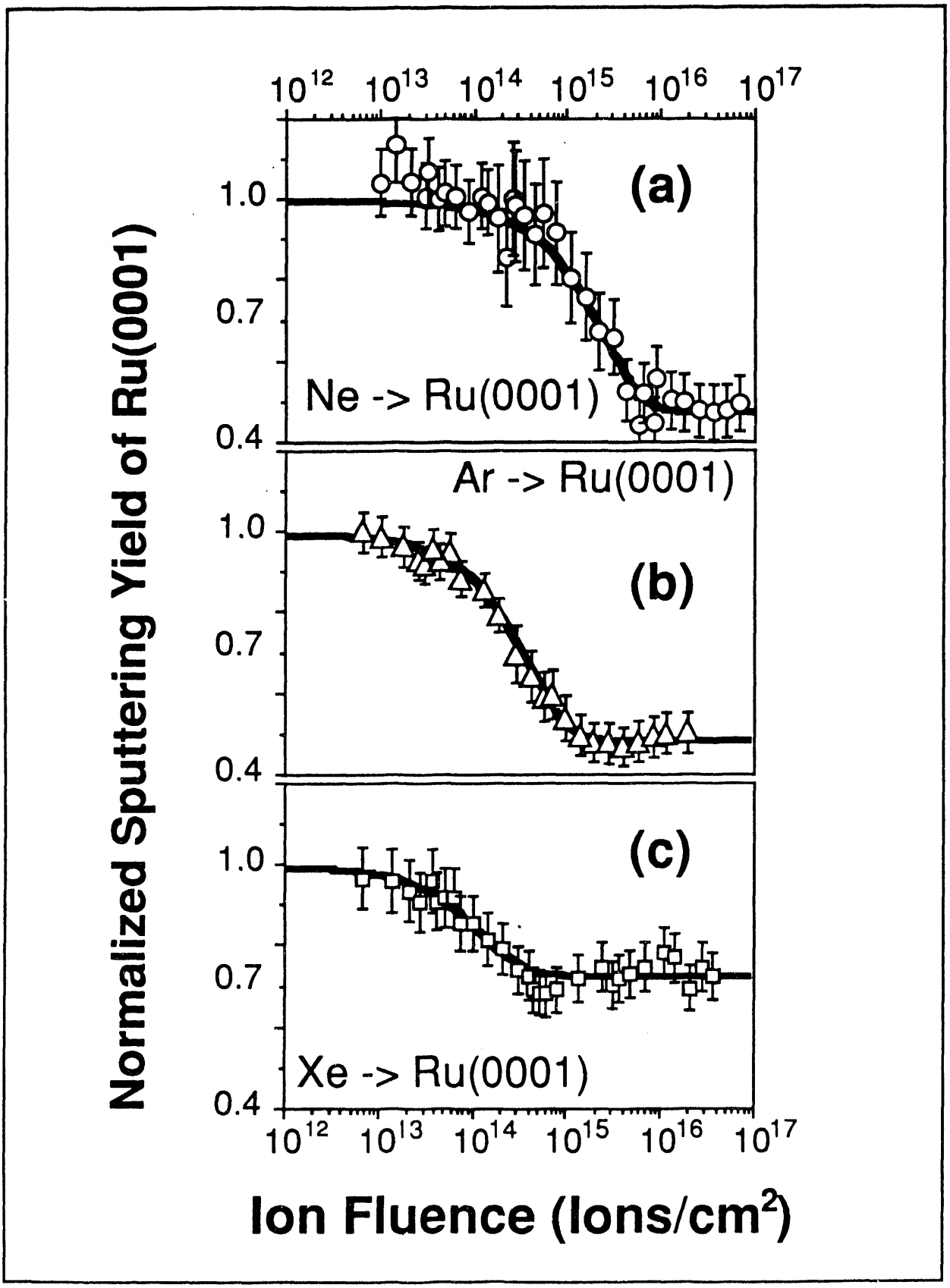
Normalized Sputtering Yield of Ru(0001)
10^12 10^13 10^14 10^15 10^16 10^17
1.0
0.7
0.4
(a)
Ne -> Ru(0001)
Ar -> Ru(0001)
(b)
(c)
Xe -> Ru(0001)
Ion Fluence (Ions/cm^2)

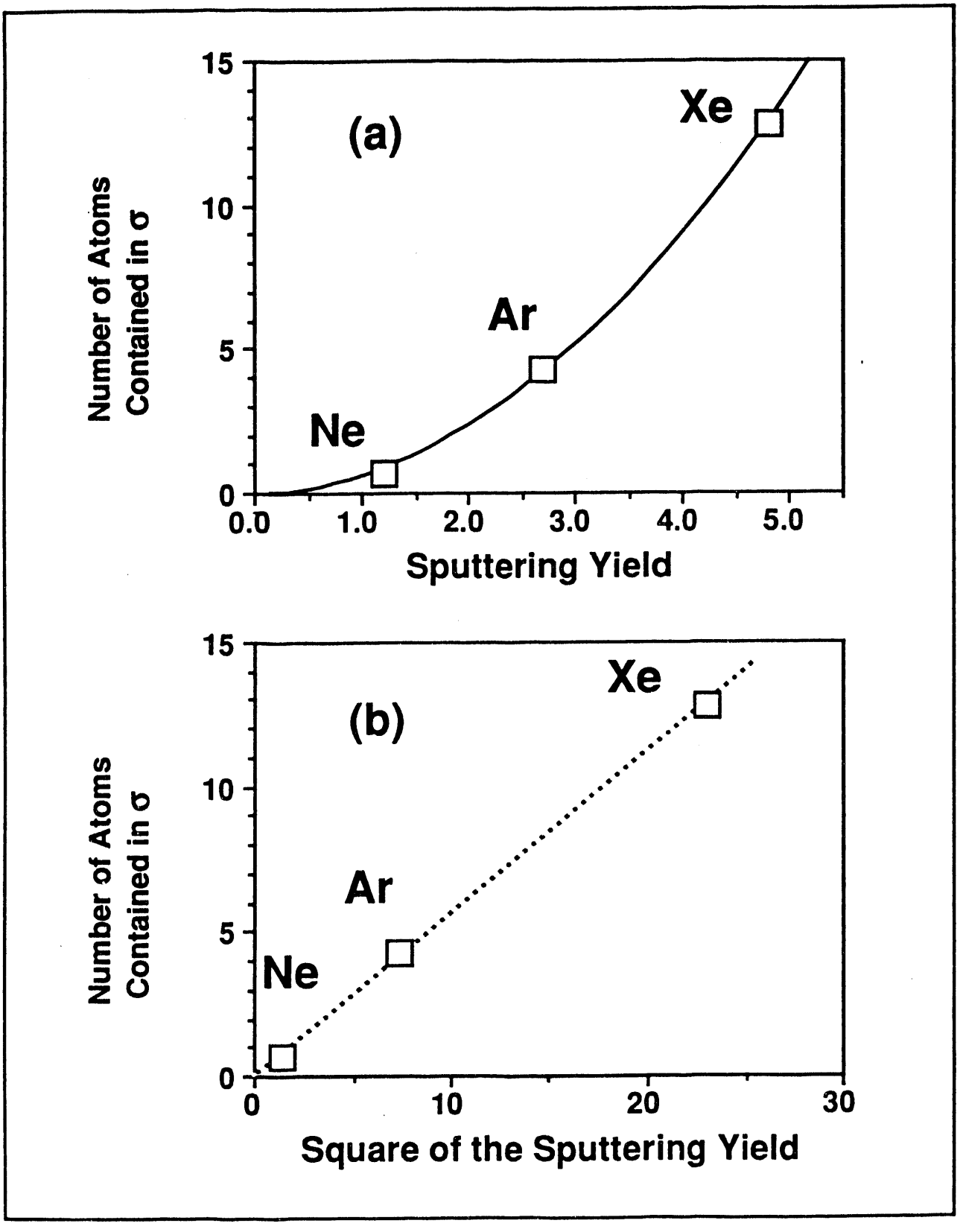
(a)
Number of Atoms Contained in σ
15
10
5
0
0.0
1.0
2.0
3.0
4.0
5.0
Sputtering Yield
Ne
Ar
Xe
(b)
Number of Atoms Contained in σ
15
10
5
0
0
10
20
30
Square of the Sputtering Yield
Ne
Ar
Xe

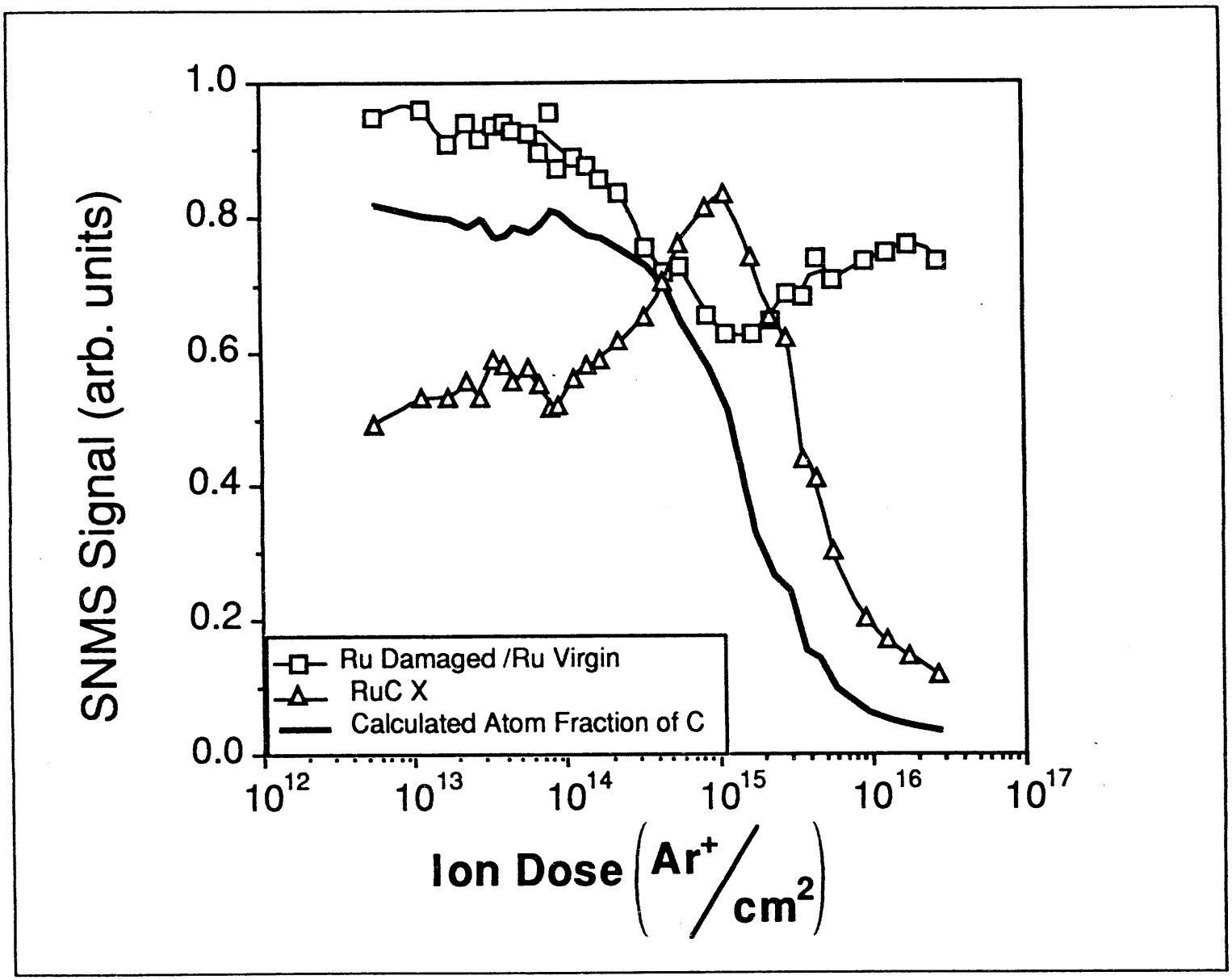
SNMS Signal (arb. units)
1.0
0.8
0.6
0.4
0.2
0.0
Ru Damaged /Ru Virgin
RuC X
Calculated Atom Fraction of C
10^{12}
10^{13}
10^{14}
10^{15}
10^{16}
10^{17}
Ion Dose $\left(Ar^{+}/cm^{2}\right)$

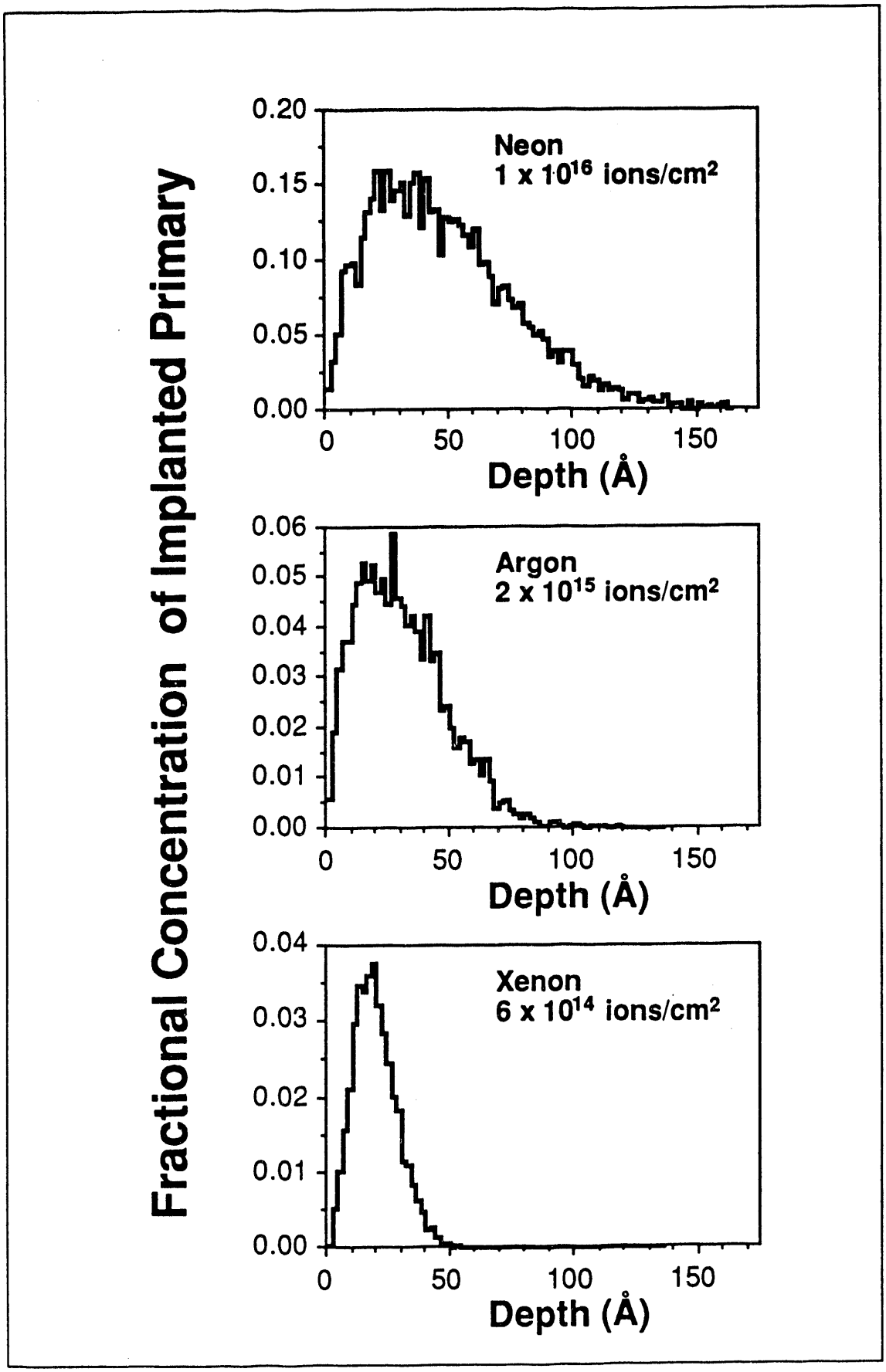
Fractional Concentration of Implanted Primary
Neon
1 x 10^16 ions/cm^2
0.20
0.15
0.10
0.05
0.00
0
50
100
150
Depth (Å)
Argon
2 x 10^15 ions/cm^2
0.06
0.05
0.04
0.03
0.02
0.01
0.00
0
50
100
150
Depth (Å)
Xenon
6 x 10^14 ions/cm^2
0.04
0.03
0.02
0.01
0.00
0
50
100
150
Depth (Å)

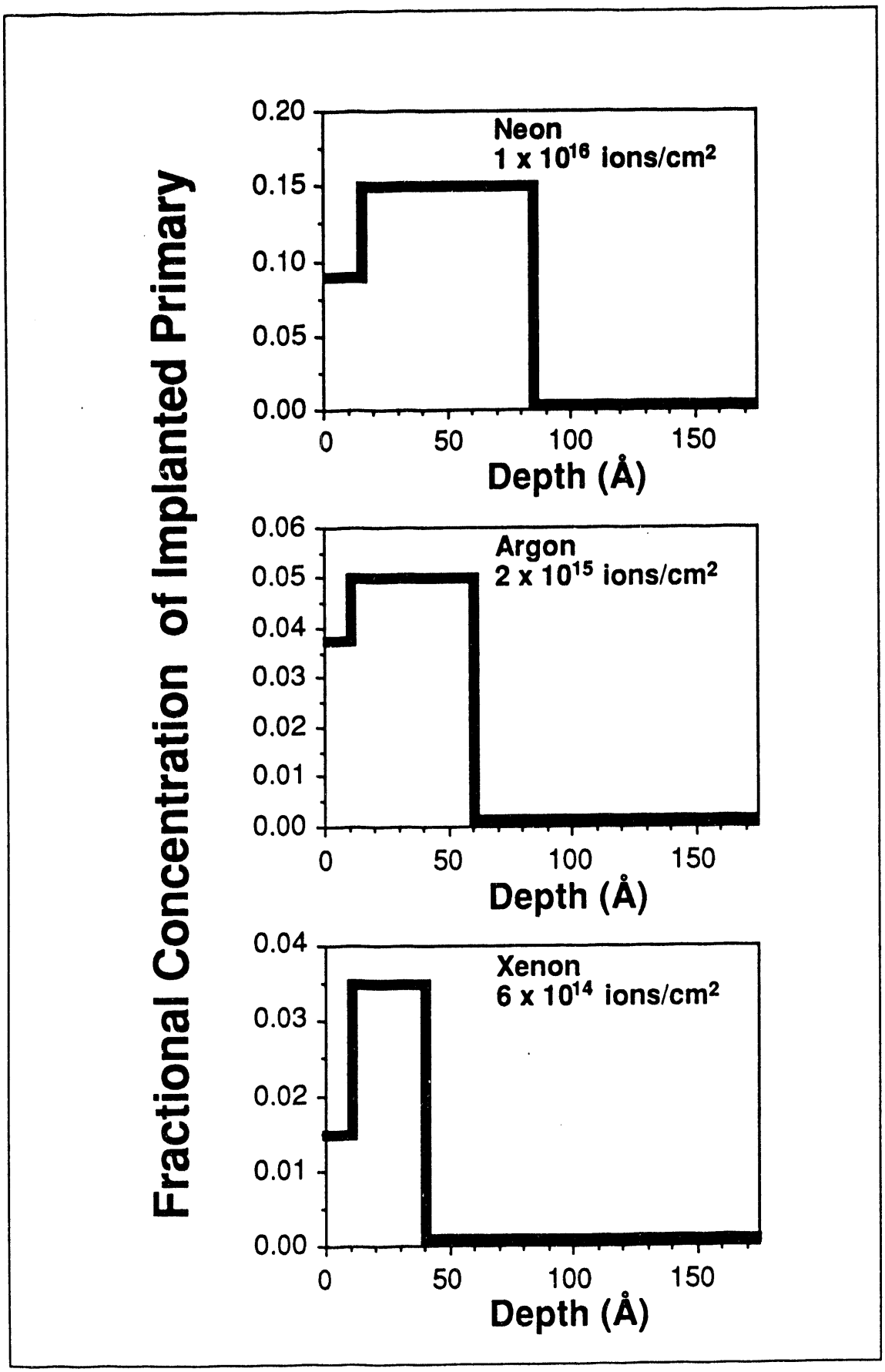
Fractional Concentration of Implanted Primary
Neon
1 x 10^16 ions/cm^2
0.20
0.15
0.10
0.05
0.00
0
50
100
150
Depth (Å)
Argon
2 x 10^15 ions/cm^2
0.06
0.05
0.04
0.03
0.02
0.01
0.00
0
50
100
150
Depth (Å)
Xenon
6 x 10^14 ions/cm^2
0.04
0.03
0.02
0.01
0.00
0
50
100
150
Depth (Å)

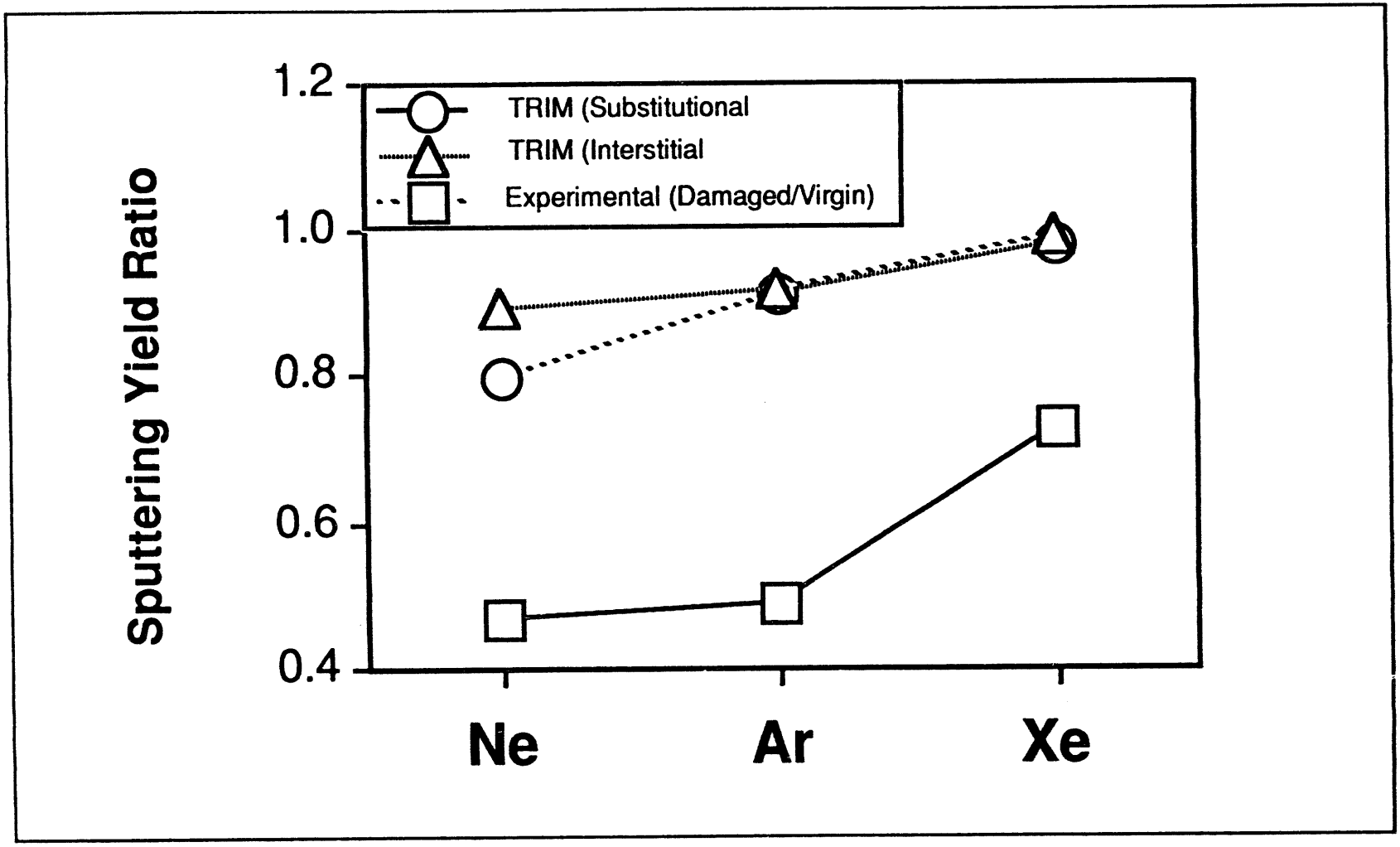
Sputtering Yield Ratio
1.2
1.0
0.8
0.6
0.4
TRIM (Substitutional
TRIM (Interstitial
Experimental (Damaged/Virgin)
Ne
Ar
Xe

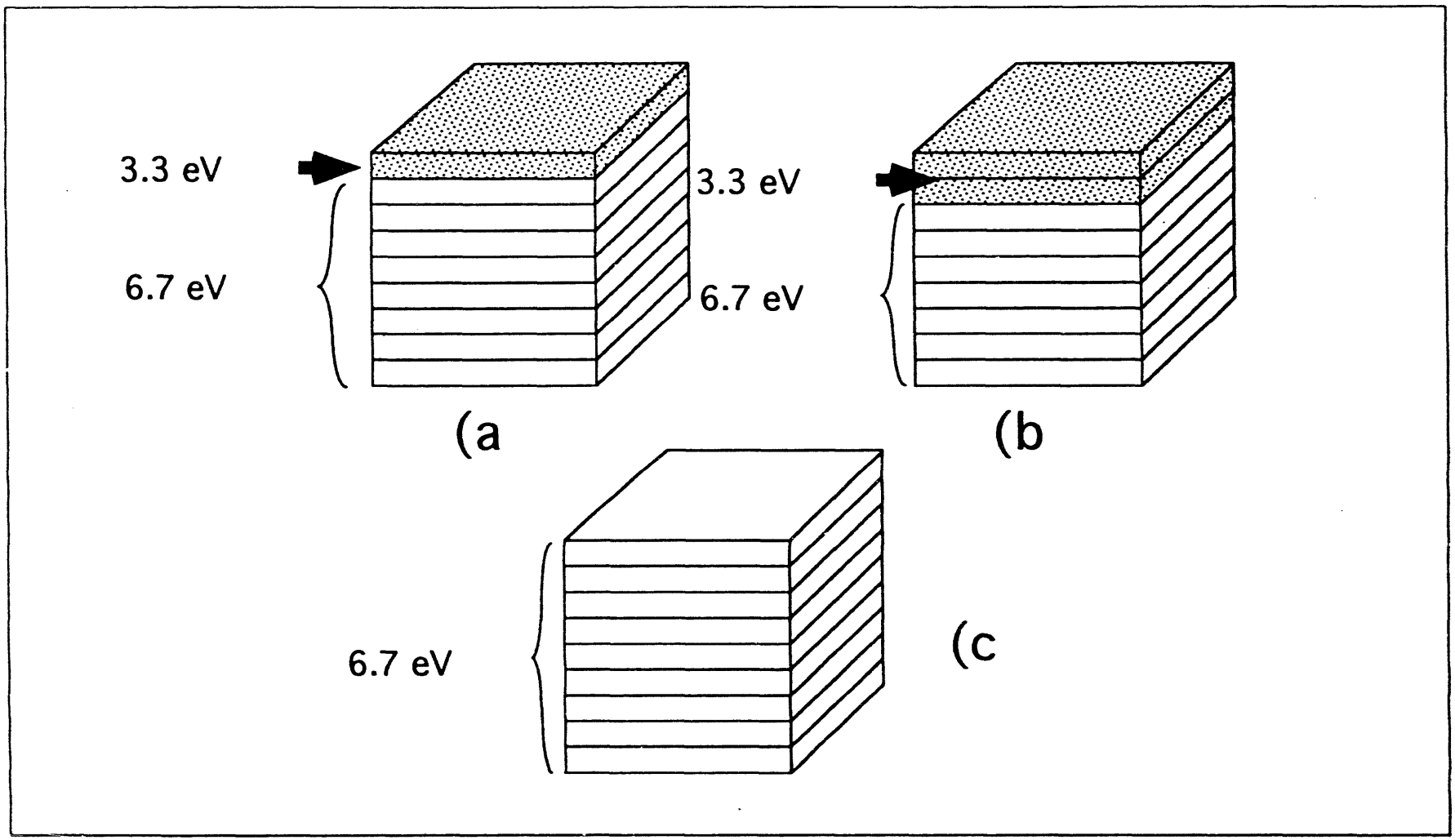
3.3 eV
6.7 eV
3.3 eV
6.7 eV
(a
(b
6.7 eV
(c

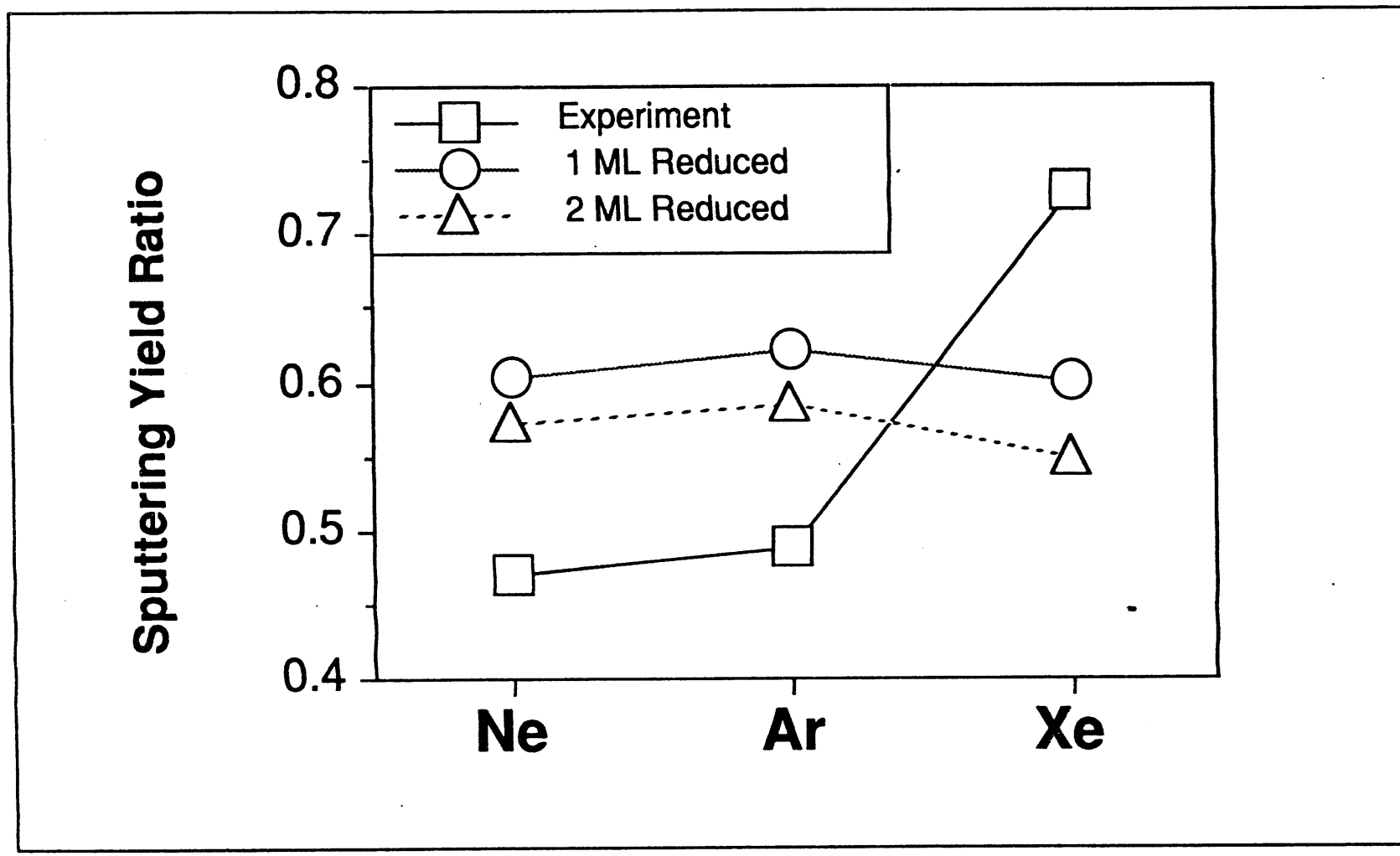
Sputtering Yield Ratio
0.8
0.7
0.6
0.5
0.4
Experiment
1 ML Reduced
2 ML Reduced
Ne
Ar
Xe

DATE
FILMED
5/12/94
END